

FlexCache: Flexible Approximate Cache System for Video Diffusion

Desen Sun, Henry Tian, Tim Lu, and Sihang Liu
University of Waterloo

Abstract

Text-to-Video applications receive increasing attention from the public. Among these, diffusion models have emerged as the most prominent approach, offering impressive quality in visual content generation. However, it still suffers from substantial computational complexity, often requiring several minutes to generate a single video. While prior research has addressed the computational overhead in text-to-image diffusion models, the techniques developed are not directly suitable for video diffusion models due to the significantly larger cache requirements and enhanced computational demands associated with video generation.

We present FlexCache, a flexible approximate cache system that addresses the challenges in two main designs. First, we compress the caches before saving them to storage. Our compression strategy can reduce $6.7\times$ consumption on average. Then we find that the approximate cache system can achieve higher hit rate and computation savings by decoupling the object and background. We further design a tailored cache replacement policy to support the two techniques mentioned above better. Through our evaluation, FlexCache reach $1.26\times$ higher throughput and 25% lower cost compared to the state-of-the-art diffusion approximate cache system.

1 Introduction

Generative models have transformed content creation by enabling the generation of high-quality images or videos through user prompts. Diffusion models have emerged and attracted the most attention [14, 17, 21, 22, 27, 59]. One of the prominent applications of these models is video generation, which has been extensively adopted in commercial platforms [2, 13, 24, 33, 45]. In the text-to-video generation, given a text prompt describing the content, a diffusion model starts with Gaussian noise and then continuously predicts and eliminates the noise over a number of denoising steps. Such a process requires hundreds of convolution and transformer operations before generating the final video, bringing a huge computation overhead and time cost.

A variety of studies have been aiming to improve the performance of diffusion models. For example, there have been parallelization approaches that divide the whole generation task into several patches and dispatch them to multiple GPUs [16, 28]. Cambricon-D [25] quantizes the differential values from adjacent diffusion steps to an extremely low-bit representation, allowing for fast processing. Although these optimizations reduce the latency of video generation, the diffusion model is still compute-intensive and takes a long time to be processed on expensive GPUs. This is especially challenging for text-to-video diffusion models. For example, using the most popular text-to-image diffusion model Stable Diffusion-XL [36] to generate a high-quality image only takes an A100 GPU 8 seconds. In comparison, the text-to-video model VideoCrafter2 [7] takes an A100 4 minutes to generate a high-quality seconds-long video.

Alternative to optimizing models, another approach is to start the generation from partially computed results rather than the initial Gaussian noise. Recent work on text-to-image diffusion models, NIRVANA, has proposed an approximate caching technique that saves the latent states (i.e., intermediate results during computation) of a few key steps in a vector database [3]. Because of the step-by-step denoising algorithm, the latent state from a later step is closer to the final output. If an incoming prompt is similar to one of the previously cached prompts (i.e., a cache hit), it loads its saved latent state as the starting point to process the new prompt and skip the cached steps. In addition, a higher prompt similarity allows a later step to be chosen. Text-to-video diffusion models also perform step-by-step denoising. However, we find that the existing caching approach does not directly apply to video generation. We identify two main challenges that stem from the key differences between image and video generation.

The first challenge comes from the cache size. Videos are much larger than images as they contain a sequence of frames. The same capacity explosion applies to latent states — the latent state cache of a 64-frame video takes $64\times$ higher capacity than an image under the same resolution. Therefore, the same storage capacity can only cache latent states of much

fewer video-generation prompts, leading to a lower hit rate. For example, according to NIRVANA, a 100 GB cache saves 18% computations but it requires 6.4 TB to achieve the same savings in video generation.

The larger size of videos inherently results in significantly higher computational complexity. As illustrated in the aforementioned example, generating a 64-frame video takes around $30\times$ longer than producing a single image of the same resolution. In the case of lightweight caching mechanisms for image diffusion, like the one from NIRVANA, are designed to maintain efficiency, as image generation typically takes only a few seconds. However, for video diffusion models, the trade-off shifts towards optimizing caching strategies. Enhancements in cache design for video diffusion models can yield substantial savings, as any improvement in the cache hit rate directly reduces its computation overhead. Consequently, the second challenge lies in designing an effective caching system to address the computational complexity of video diffusion models.

This work aims to enable efficient approximate caching for text-to-video diffusion models. Our system, FlexCache, incorporates two core techniques aimed at reducing cache size and enhancing cache hit rates. Our analysis reveals that the inherent similarity within latent states offers significant potential for compression. We identify two types of similarities. First, inter-frame similarity is evident, where certain frames exhibit redundancy. Drawing inspiration from prior research on video processing [15, 56], which identifies and deduplicates similar frames, we observe that analogous patterns exist in latent states, allowing the retention of only unique key frames. Second, we observe that objects and their movements in the final video remain consistent throughout denoising steps. Consequently, the differential values between frames (i.e., differences) effectively represent identical movements across all denoising steps, making them suitable for compression. By leveraging these compression opportunities, FlexCache integrates key frame compression to achieve $6.7\times$ cache size reduction, with minimal impact on video quality.

To enhance the cache hit rate, we propose a caching mechanism specifically designed for text-to-video diffusion models. Instead of solely relying on the complete prompt for cache lookups, we find that decoupling object and background and performing separate lookups allow for 13.8% higher hit rate. Building on this insight, FlexCache incorporates text extraction along with object and background segmentation to reuse cached latent states from videos with the most similar object or background. Depending on the similarity, FlexCache dynamically selects between the whole prompt cache or combining object and background caches. Additionally, we design a novel cache replacement policy tailored to our compressed and decoupled caching scheme. It holistically accounts for the capacity of cached video latent states, cache access recency, and cache access frequency.

We evaluate FlexCache using VideoCrafter2 [7] as the

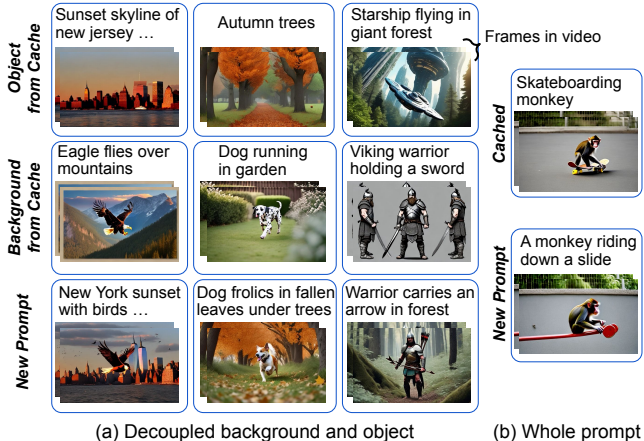


Figure 1: Example of FlexCache generations.

text-to-video diffusion model and VidProM [52] as the video prompt dataset, on a GCP instance with an A100 GPU. Figure 1a and 1b demonstrate video generations (the first frame) from the decoupled object and background caches and the whole prompt caches in FlexCache, respectively. In both modes, FlexCache achieves high quality. We summarize the contributions as follows:

- We design a cache compression technique that leverages similarities in video diffusion models, allowing efficient latent state caching with almost no degradation in the quality.
- We propose a cache lookup mechanism that decouples the object and background from the whole prompt to achieve a higher hit rate. We further design a new cache replacement policy tailored for video latent state caching that incorporates computations savings, cache size, and recency.
- We incorporate these techniques in LRBUs that reuses latent states for text-to-video diffusion models.
- We evaluate FlexCache with a real-world dataset and a baseline that adapts NIRVANA’s image caching to video cache. FlexCache with a 1000 GB cache storage improves the throughput by 26% and saves 25% cost on average over this baseline, with almost no degradation in video quality.

2 Background and Motivation

In this section, we first introduce diffusion models and approximate caching, and then present the challenges in optimizing video diffusion models.

2.1 Diffusion Model

Diffusion models are a class of generative models that generate the image [36, 43] or video [5, 7] from prompts. Recent research has demonstrated that diffusion models achieve better performance than previous generation models on vision tasks [14]. These models generate the output by taking a

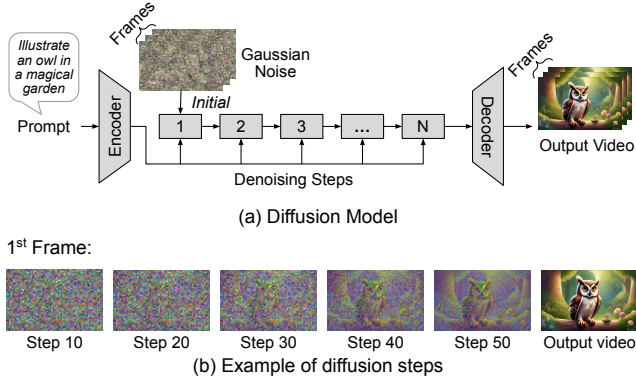


Figure 2: Diffusion model for video generation.

prompt and an initial Gaussian noise, and then eliminate unnecessary noise. The denoise procedure takes multiple steps, making diffusion model computation intensive. Text-to-image diffusion and text-to-video diffusion have similar architectures, the primary difference is that image generation only applies one dimension transformer, while video tasks usually deploy spatial-temporal transformers [49, 53] to strengthen the interaction between spatial and temporal perceptions.

Figure 2a illustrates the structure of a diffusion model. It takes Gaussian noise as the initial input and then goes through multiple denoising steps, where the output from the prior step is taken as the input to the next. Each step processes the current noise and the embedding generated by the given prompt to predict the noise, and eliminate such noise from the input. After a number of steps, the noise is reduced and can be recovered to a high-quality video by decoder. The denoising part is the core component in diffusion models, typically based on U-Net [5, 7, 44] or Transformer (DiT) [8, 33, 35]. Figure 2b demonstrates this process in video generation, where the noise gradually reduces and eventually becomes the final video over 50 denoising steps. To alleviate the heavy computation complexity, previous research finds a way to infer diffusion model in latent space [43]. We can see that although the quality increasingly gets better with step growth, the position of that owl never moves within the same frame.

Diffusion models are costly as they take multiple steps to get the final output. There have been optimizations on the sampler to decrease the number of steps in diffusion models, such as decreasing the number of steps to 100 [19], 50 [46], and 20 [30]. These steps need to be processed in sequence, which occupies the majority overhead of diffusion models. There have also been works that split the input to multiple patches [16, 28], or schedule different modules in diffusion such as LoRA [20], ControlNet [61] to suitable devices [29], to achieve higher parallelism within each step, reducing the latency. Although these proposals improve performance, the root problem of high compute complexity remains.

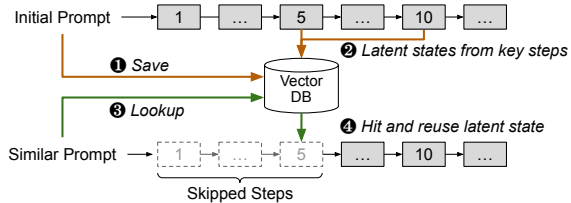


Figure 3: Approximate-caching for diffusion models.

2.2 Caching for Diffusion Models

To relieve the costly computation overhead, one solution is to store the latent states (i.e., intermediate states during step-by-step computation) in a cache and load them to skip steps when a similar prompt arrives [3, 18]. The similarity between the incoming prompt and the cached prompt determines the computations that can be saved.

NIRVANA [3] is the state-of-the-art work that adopts approximate cache to reduce computation in text-to-image diffusion models. As illustrated in Figure 3, upon a new request, NIRVANA saves the prompt ① and latent states ② of key steps (5th, 10th, 15th, 20th, and 25th) in a cache. The cache is based on a vector database to enable lookup. Given a new prompt, NIRVANA attempts to look up ③ the most similar previous prompt using cosine similarity as the metric. If a cache is hit, the current request can set this cache as input ④ (the 5th step in this example) and proceed from the next step. The higher the prompt similarity score is, the more steps the incoming prompt can skip. NIRVANA has shown that the cached prompt can save up to 25 steps out of a total of 50 steps. Because the remaining steps continue to process the latent state, the output quality remains good as the diffusion model takes additional steps to continue the update.

Caching is a promising solution to reduce computation cost, as NIRVANA has demonstrated in image generation. However, caching is not a one-size-fits-all solution to diffusion-based generation. The process of generating videos via diffusion models is similar to that of images. Straightforwardly adapting approximate caching, nonetheless, cannot reap the same benefit. Next, we describe the challenges in enabling caching for video generation.

2.3 Challenges in Caching Video Generation

Cache hit rate and similarity scores are the two key aspects of approximate caching — a high cache hit rate enables a larger number of prompts to reuse caches, while a high similarity score allows prompts to skip additional steps. However, achieving a high hit rate and a high similarity score simultaneously is challenging. Unlike image generation models, video generation models feature substantially larger latent state sizes and higher computational complexity. We next explain these key differences in detail.

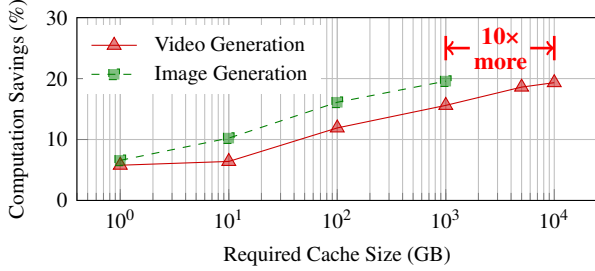


Figure 4: Cache size required to achieve different levels of computation savings, for both image and video generations.

Larger latent states. Typical video generation applications allow users to generate seconds-long videos [24, 33], which consist of tens to hundreds of frames. For example, one 64-frame video of resolution 320×512 with each pixel defined by 4 channels (RGBA) has a total size of $320 \times 512 \times 4$. The latent state is downsampled by $8 \times$ but still has a size of $40 \times 64 \times 4$. This dimension leads to 2.5 MB of latent state size. Directly adapting the caching scheme in NIRVANA takes a total capacity of 12.5 MB to save the five key steps (5th, 10th, 15th, 20th, and 25th) of each prompt. In contrast, images are static, consisting of only a single “frame”. Thus, caching the latent states of the image with the same dimension only requires 200 kB. We demonstrate the capacity challenge using the VidProM dataset [52] that comes from real user prompts (more methodology details in Section 6.1). We evaluate an experiment with infinite storage and present the certain computation savings (y-axis) and the corresponding cache requirements (x-axis) in Figure 4. To achieve 19.3 % computation savings, the cache capacity requirement is 10 TB. Theoretically, generating images using identical prompts would require $10 \times$ less cache compared to video generation when employing the same resolution as NIRVANA—significantly higher than videos. As video diffusion models become increasingly widespread, we expect the capacity demand to exacerbate as models scale.

Higher computational complexity. As one video consists of a sequence of frames, each diffusion step takes a more complex procedure than image generation. Different from image generation which only applies 2D convolution and spatial transformer, video generation adds another dimension — temporal dimension for both convolution and transformer operations. As a result, using VideoCrafter2 to generate a 64-frame video of 320×512 resolution takes 242 seconds on an A100 GPU, whereas generating an image of the same resolution only takes 8 seconds using the Stable Diffusion-XL model [36]. On the other hand, savings from caching allow the diffusion model to skip steps, which proportionally reduces the total generation time. For example, skipping 10 steps means 48 seconds for video generation while it only translates to 1.6 seconds for image generation. This stark

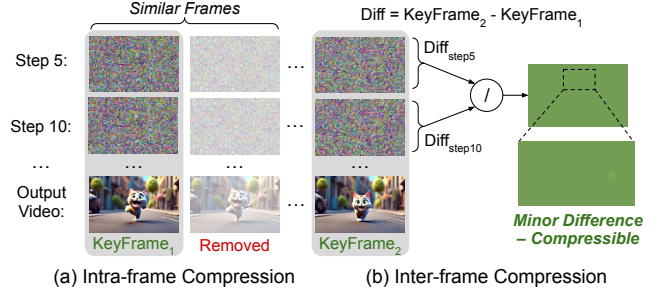


Figure 5: Example of intra-step and inter-step compression.

difference in time scale indicates that the tradeoffs between caching performance and the complexity of the cache system have been reversed. In image diffusion caching, a lightweight caching lookup system is required as generating a single image only takes a matter of seconds. However, the high potential benefit in absolute time savings of video diffusion models motivates further optimizations in caching design for a higher hit rate and similarity score.

These challenges highlight the need for a more efficient caching scheme for text-to-video diffusion models. This work aims to redesign approximate caching by overcoming challenges that stem from the high latent size and high computational complexity. Next, we will present the high-level ideas.

3 Overview of FlexCache

To overcome the aforementioned challenges, we proposed FlexCache to achieve efficient caching for video diffusion models. We start with describing the high-level ideas and then present an overview of FlexCache.

3.1 High-level Ideas

3.1.1 Cache Compression

The large size of the latent cache is due to video frames. Nonetheless, the inherent similarity in latent states provides an opportunity to compress the cache size, and save more latent states in the cache. We observe two types of similarities. The first type is the similarity among frames. Some works point out that there are redundant frames in a video, allowing them to discard similar frames [15, 56]. They inspire us that we can try to leverage the frame similarities in latent noise. Changes in a video do not happen suddenly but rather gradually. Therefore, repeated frames can be removed to reduce the cache size, without degrading the quality. And, only a few *key frames* need to be preserved. Figure 5a is an example video of a “walking cat”, where the first two frames are almost identical and the second one can be removed from the cache. As diffusion models gradually reduce noise over steps, the same similarity among frames also exists across latent states. This

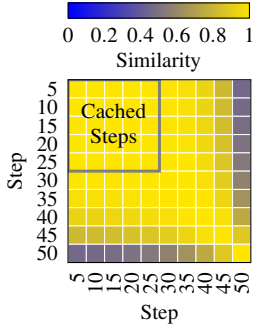


Figure 6: Differential value similarity among steps.

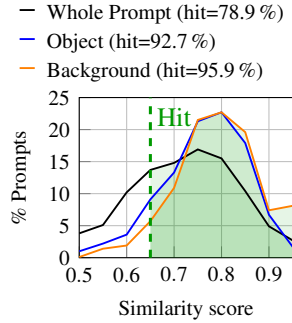


Figure 7: Whole prompt, object, and background hit rates.

type of similarity enables compression within each step. We refer to this compression technique as *intra-step compression*.

The second type of similarity is the differential value similarity. We find that even though diffusion models reduce the noise of latent states over steps (as demonstrated in Figure 2), the same frame among steps has the same content, following the same movement. In comparison, key frames within the same step have major changes as the scene of the video changes. Following this observation, if we obtain the difference between two key frames (i.e., calculate their differential value) and compare them among steps, there should be minimum differences. Figure 6 presents the average similarity scores for these differential values from 5k videos. It is clear that the differential values are almost identical within the first 25 steps, i.e., the steps to be cached. Although the differential tends to be more dissimilar with step growth, it’s useless to store the later several latent states according to NIRVANA. Figure 5b demonstrates this observation. We calculate the differential ($Diff$) among $KeyFrame1$ and $KeyFrame2$ for both 5th step and 10th step, i.e., $Diff_{step5}$ and $Diff_{step10}$, respectively. Then, we calculate the ratio between $Diff_{step5}$ and $Diff_{step10}$, ending up with an image with almost all pixels identical, except for a few pixels as shown in the zoom-in view. The ratio between differential frames can therefore be represented with a single floating point value, eliminating the need for saving all key frames. We refer to the second compression technique as *inter-step compression*.

Together, the two compression techniques can reduce the video latent cache size by an average of $6.7\times$, with almost no degradation in the video quality. We explain the details about the cache compression in Section 4.1.

3.1.2 Cache Hit Rate

Previous studies, such as NIRVANA, compare the whole prompt’s similarity with others, and choose the most similar existing prompt’s cache as the input. It’s always too strict to find another prompt that describes exactly the same thing as the current prompt. However, we found that the prompts of video generation requests always consist of two parts: the

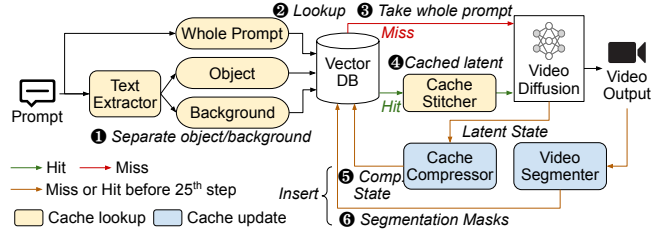


Figure 8: Overview of FlexCache.

background and the object. This observation enables us to decouple the cache lookup.

Figure 7 shows the distribution of prompts that have certain similarity scores. We assume that there is a pool of 100k requests that have been served and then we track the cosine similarity for the next 1k prompts with the existing 100k prompts. We use a transformer-based text extractor to help us extract the key contents of the background and object from a given prompt. For background and foreground sentences, we also convert them to CLIP embeddings [40] and get their similarity scores. Based on NIRVANA, the state-of-the-art approximate cache research in the diffusion model, requests can reuse the intermediate states only when their similarity score is over 0.65. The higher their similarity score is, the more computations the request can save. By decoupling the object and background from the whole prompt, the cache system achieves at least 13.8% higher hit rate.

Finally, we incorporate a novel cache replacement policy in our caching system. This policy takes account of both memory and recency which is ignored by NIRVANA. Besides, unlike NIRVANA, which only inserts cache when cache misses, we attempt to insert the cache no matter if it skips steps.

3.2 System Overview

The cache compression and hit rate optimization aim to save more steps in video generation. Putting these ideas together, Figure 8 shows the overview of FlexCache. We divide the process into two phases: cache lookup and cache update.

Cache lookup. When a new request arrives, a *text extractor* separates the object and background description ①. Then, FlexCache converts both the extracted prompt (*object + background*) and the *whole prompt* into embeddings using a CLIP model [40] and looks them up in a vector database (Vector DB) ②. The Vector DB caches latent states in 5 key steps: 5th, 10th, 15th, 20th, and 25th, similar to NIRVANA’s strategy; it maintains three indices for lookup, corresponding to the whole prompt, the object part, and the background part. All indexing structures share the same cached latent states. The lookup is a hit if there is at least a pair of object + background or a whole prompt cache that is similar to the incoming prompt

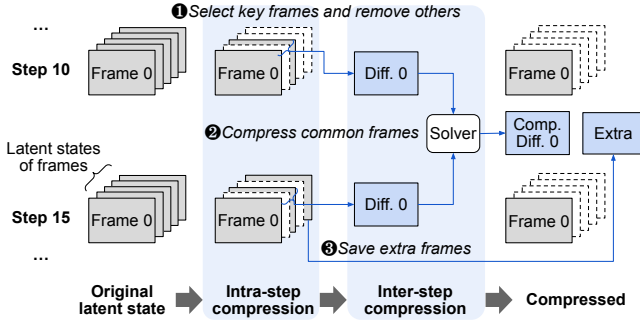


Figure 9: Overview of Cache Compressor.

(similarity threshold is 0.65, following NIRVANA); otherwise, it is a miss. Note that having only the object or background pass the similarity threshold is not regarded as a hit because video generation requires both. FlexCache’s cache selection prioritizes the one with the highest similarity with the incoming prompt. We discuss the selection details in Section 4.2.1. In the case of a *miss* ③, the video diffusion model processes the original prompt; in the case of a *hit* ④, the diffusion model starts with the cached latent state and thus takes fewer denoising steps. A *cache sticher* combines the decoupled object and background caches when they have better similarity.

Cache update. When the video has been generated, FlexCache saves its latent state back to the Vector DB if the prompt was a miss or the cached step was before the 25th step (indicating a need for a better cache to serve future prompts that akin). If FlexCache generates the video from the cache, then the latent states after the initial input (the reused cache) will be saved. A *cache compressor* compresses the states ⑤ (details in Section 4.1). In parallel, a *video segmenter* generates a segmentation mask for each frame of the output video, depicting the boundary between the object and the background ⑥ (details in Section 4.2.2). Finally, FlexCache inserts both the compressed latent states and the segmentation masks into the Vector DB for future prompts to look up.

4 Design of FlexCache

In this section, we describe the design of FlexCache in detail, including the cache compression mechanism and optimization strategies that enable a higher hit rate.

4.1 Cache Compression

We use a combination of intra- and inter-step compression techniques to reduce the size of cached latent states, allowing for more cached saved and achieving a higher hit rate. Figure 9 illustrates the workflow of this compression technique. Assuming that there are two latent states and each latent state

has five frames. In the intra-step compression stage, we select and save only the key frames ①. A total of five frames that are similar to others are discarded after this stage. Then, inter-step compression further reduces the size of key frames’ latent states with a solver that reduces differential values of the common key frames ②. Note that not all the latent states have the same number of key frames, so there can be extra frames after inter-step compression. We save them as extra frames ③. Eventually, the original ten frames are reduced to only four. Next, we describe both techniques in detail.

4.1.1 Intra-step Compression

We first propose a latent state compression mechanism by leveraging the frame similarity. Unlike ground truth video compression, which needs to maintain the same quality after decompression, such latent states are still supposed to be processed for multiple steps, allowing for a certain degree of accuracy loss. So it’s possible to only save the key frames and simply repeat these frames when recovering.

We try to traverse the whole latent state from the last frame to the first frame when compressing. We get the similarity scores with the current frame and all the frames in front of it. Then we set a threshold to ensure that all of the other frames share enough similarities with the key frames. The detail of the threshold will be discussed in Section 5. Next, we record the map relationship of the key frame and the compressed frame. If there are no other similar frames, then the current frame is also one key frame and it will map to itself. Finally, the original frame will be removed if it is not a key frame. In this way, we eliminate all of the unnecessary frames and only save the key frames and the relationship with the key frames, which take much less storage than the whole latent state. Figure 14b shows the average percentage of redundant frames. With steps growing, the frames become less similar since there are more details within frames. When decompression, we can simply traverse the map and repeat the key frames to other positions. Although it is not exactly the same as the original latent state, the accuracy loss is acceptable because there are still some computations, which will not hurt the final quality. We will show the detailed evaluation in Section 6.2.4.

4.1.2 Inter-step Compression

We further design a compression mechanism based on the observation that the differential values among steps are also similar. For each cached denoising step s , the differential values of the m^{th} frame are its difference from the first frame, i.e., $Diff_s^m = Frame_s^m - Frame_s^0$. Based on the insight in Section 3.1.1, it is possible to use the set of differential values of all key frames from one step (which we refer to as the *base Diff_{base}*) to calculate those from other steps, effectively reducing the storage size. Note that some steps may have more key frames, which will be separately saved as extra frames

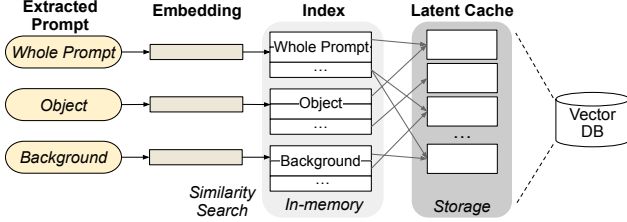


Figure 10: Vector database for cache lookup.

in the cache. The value that will be used to generate other differential values from the *base* is defined as α_s . As there are 5 cached steps in FlexCache, we have a total of 5 candidates for $Diff_{base}$. The inter-step compression mechanism will attempt each of them and choose the one that leads to the highest similarity after decompression. We next explain the calculation for α_s .

We further denote i, j as the i^{th} row and j^{th} column pixel in a frame, and use $Diff_s$ to collectively represent each key frame $Diff_s^m$ within step s . Because $Diff_s$ and $Diff_{base}$ are known before compression, we model this as an inverse problem that infers model parameters from relevant observations. Here we treat the $Diff_s$ and $Diff_{base}$ as the measurements and α_s is the parameter that needs to be inferred. The inverse problem can be formulated as finding a solution to the operator equation $K(u) = f$, where K is the forward operator, u is the existing frame and f is the measurement. We therefore can define our equation as:

$$K(Diff_{base}) = Diff_s \quad (1)$$

As Figure 5 and 6 indicate the relationship between multiple differential values follows a linear-like pattern, the goal is to find the coefficient α_s that minimizes the average difference between $\alpha_s \times Diff_{base}$ and $Diff_s$. Thus the inverse goal is to minimize $\sum_{i,j}^{Diff^m} (Diff_s^{m,i,j} - Diff_{base}^{m,i,j} \times \alpha_s)^2$. This minimization is a standard least squares problem. We take the derivative of α_s and calculate its value when the derivative equals 0. Finally, we derive this forward operator:

$$K(Diff_{base}^m) = \frac{\sum_{i,j}^{Diff^m} (Diff_s^{m,i,j} \times Diff_{base}^{m,i,j})}{\sum_{i,j}^{Diff^m} (Diff_{base}^{m,i,j})^2} \times Diff_{base}^m \quad (2)$$

The coefficient of the forward operator can be represented in a single value that occupies much less memory. In this way, we leverage the similarity across denoising steps to further compress the cache.

4.2 Cache Hit Rate Optimizations

In this section, we will describe our cache design that optimizes for cache hit rate through decoupled object and background lookup and latent reconstruction, and a tailored cache replacement policy.

4.2.1 Cache Lookup

We find that both prompt [9, 47] and the final video [4] can be decoupled into two parts: the object that usually shows the main character or the event, the background that usually describes the general environment or settings.

Based on this insight, we propose an object-background segmentation technique to achieve a higher hit rate and more computation savings. Figure 10 demonstrates our design. For an incoming prompt, a text extractor first extracts the descriptions of the object and the background from the original prompt. The vector DB maintains three index tables to look up the three kinds of prompts. The index tables are not memory-consuming and thus are kept in memory but the latent states are saved in storage. Next, FlexCache looks up the original prompt and the extracted object and background prompts in the vector DB to find their most similar prompts, and get 3 similarity scores: $Sim_{background}$, Sim_{object} , and Sim_{whole} . Then it chooses the higher value from Sim_{whole} and $\min(Sim_{background}, Sim_{object})$, to skip more steps. When $\min(Sim_{background}, Sim_{object}) > Sim_{whole}$, applying the background-object segmentation will yield more computation savings. We show the fraction of hits from the whole prompt, and decoupled object and background prompts in Section 6.2.2.

4.2.2 Video Latent Reconstruction

When FlexCache finds latent caches with higher similarity scores with the decoupled object and background descriptions than the whole prompt, the cache returns the latent states of the two videos: one provides the object and another provides the background. Next, FlexCache needs to stitch these two caches into one as the input to the video diffusion model.

Simply getting the average value of these two latent states does not work well because both frames contain unneeded pixels. To precisely identify which part of the videos will be used as the object/background of the new generation, we adopt a segmentation model that takes the extracted object and background descriptions. However, latent states, especially those from the first several denoising steps, are mostly noise (as Figure 2 shows), so the segmentation model can hardly detect any objects. However, the positions of these objects are never changed as the denoising steps increase. Our approach is to segment only the final video by generating masks for objects and backgrounds, and then apply these masks to the previous latent states of the cached steps. FlexCache saves the masks along with the caches. While stitching, FlexCache restores the caches and masks of two latent states, extracts the required part from each of the latent states, and combines them into a single latent state. FlexCache will combine the two masks in case they do not perfectly align. Typically, a good prompt similarity guarantees that such misalignment is minor. After taking the remaining denoising steps, this

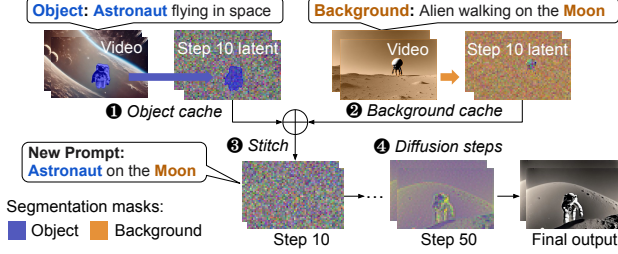


Figure 11: Illustration of cache reconstruction.

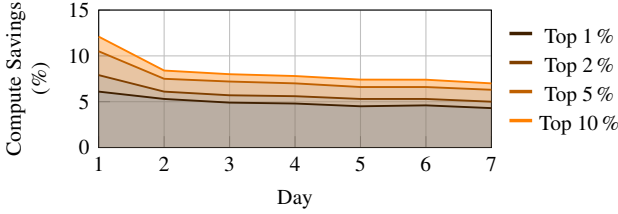


Figure 12: Compute savings from top 1% – 10% cached prompts over time.

stitching will not introduce significant quality loss. This new latent state is then taken as input to the video diffusion model.

Figure 11 demonstrates the workflow cache reconstruction. There is a new request for a video about *astronaut* on the *Moon*. The vector DB does not have a good match for the whole prompt, so it provides two caches: “*astronaut* flying in space” ① and “*alien walking on the Moon*” ②. The former provides the object and the latter provides the background component. Thus, FlexCache extracts the astronaut part from the former cache, and the moon part from the later cache using the previously saved masks to stitch them into one state ③. After stitching, the new request can proceed from the 11th step ④. The “*alien*” part in the background cache will be replaced by pixels in the object cache at the same location. This minor misalignment does not lead to any observable blurred pixels or extra objects in the final output.

4.2.3 Cache Replacement

A cache replacement policy aims to evict the least desirable cache entry in the cache upon a new insertion. NIRVANA introduces a replacement policy – Least Computationally Beneficial and Frequently Used (LCBFU) for their image caching system. It selects the cache entry that has saved the least computations. Suppose the whole cache has i cache entries, it uses $f_i \times step_i$ to determine the priority of i^{th} cache and evicts the cache with the least priority. However, we observe that video caching is in stark contrast to image caching.

Observation 1: Non-uniform cache size. The size of each cache entry (i.e., latent of video) is not constant, as the number of extra frames varies by steps or prompt. As a result,

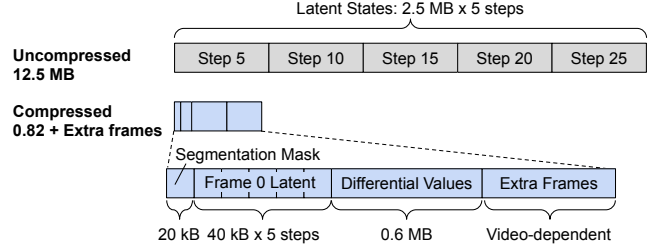


Figure 13: Memory consumption breakdown for uncompressed and compressed cache.

replacing one cache entry may lead to different benefits in storage. In comparison, the existing image cache replacement policy LCBFU only captures the performance benefits since image caching only has uniform-sized cache entries.

Observation 2: Decreasing reuse over time. Recency is equally critical for the replacement policy. We conduct an experiment based on VidProM [52], a real-world user trace dataset. We track the change of computation savings from the hottest prompts (i.e., most frequently hit) over time. First, we select the prompts that contributes top 1–10% computation savings to a single day. Then, we further collect their savings for the following days. The result is shown in Figure 12. We observe that the top 1% prompts remain popular for a long time. In contrast, top 10% prompts exhibit a noticeable decline in popularity over days. LCBFU overlooks recency and tends to save caches frequently accessed in the past but not recently reused.

LRBU: To evict caches that are less likely to be reused in the future, we propose a novel cache replacement policy named *Least Reused Benefit Unit* (LRBU), which takes both memory capacity and recency into consideration based on the observations mentioned above. LRBU treats individual step’s cache as separated cache entries and evicts one of them will not influence other caches from the same request. We define the priority of i^{th} cache as:

$$Priority_i = \frac{f_i \times step_i}{Capacity_i \times Duration_i} \quad (3)$$

where f_i denotes the access frequency of the cache, $step_i$ denotes the number of steps that can be saved, $Capacity_i$ denotes the size of the cache entry (i.e., number of frames), and $Duration_i$ represents the time elapsed since the cache was last accessed. Cache entry with the lowest *Priority* will be evicted first. Specifically, $Capacity_i$ in Equation (3) aims to normalize the benefit by its capacity; $Duration_i$ aims to evict caches that have not been reused for a long time, preventing stale cache entries that were accessed frequently in the past from staying in the cache system forever.

4.2.4 Cache Operations

The cache in FlexCache takes two operations:

Insertion. Unlike LCBFU, which only saves the cache upon a miss, the efficient latent state compression allows LRBU to save more states. When a prompt hits a cache (either whole prompt or decoupled) and the step it hits is n . If $n < 25$, i.e., the highest step that can be cached, LRBU saves the additional key steps between n and 25. If $n = 25$, then no extra states will be saved. This mechanism allows more later steps to be saved, providing more potential computation savings for future prompts that are similar to the one that was just processed.

Eviction. LRBU keeps track of all the cached latent states. LRBU updates their duration each time when it is going to start evicting and then discards enough caches until the new caches can be inserted. The eviction mechanism chooses the cache entry with the lowest *Priority* according to Equation (3). Because the latent states of the same prompt from different steps can be evicted separately, some states of certain steps may be evicted earlier, leaving a “hole”. We take the same approach as NIRVANA’s solution to the “hole” problem. If an incoming prompt hits an already evicted step from an existing prompt, FlexCache takes an earlier step instead.

4.3 Cache Entry Structure

Putting the caching compression and hit rate optimization techniques together, Figure 13 shows each component in a compressed cache entry that maintains the 5th, 10th, 15th, 20th, and 25th steps of latent states. Directly saving these 5 steps takes 12.5 MB for each prompt. FlexCache’s compression technique significantly reduces the space requirement. For each prompt, the cache entry maintains the first frame of each step, the differential value generated by the common key frames (i.e., the key frame that exists for all 5 steps), and the extra frames as some states have more key frames than others. To enable the decoupled cache lookup, the segmentation mask takes 40 kB as it takes only 1 bit for each pixel. In our evaluation, we find that the cache size can reach up to 4.9 MB, which is still much less than uncompressed. See Section 6.2.4 for detailed evaluations.

5 Implementation of FlexCache

We implement FlexCache in PyTorch [34] with 1.9k line of codes. The implementation details of components in Figure 8 are the following:

Diffusion Model. We use the industry-standard VideoCrafter2 [7] as the text-to-video diffusion model, with the integration of FreeNoise [38] to generate 64-frame videos (4 seconds). We use xformers [26], one of the most popular transformer frameworks, to help optimize the diffusion model as other projects [6, 36, 59, 62]. We follow the default

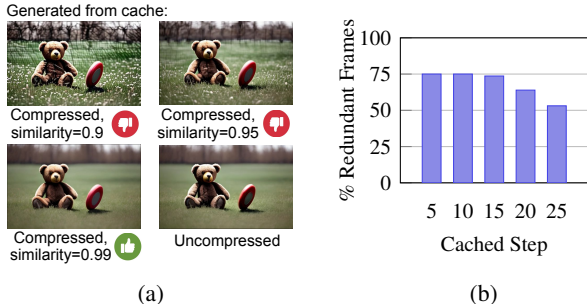


Figure 14: (a) Quality of video under different similarity levels in compression. (b) Number of redundant latent frames among steps when the similarity threshold is 0.99.

configuration of VideoCrafter2, with video resolution of $320 \times 512 \times 4$, $8 \times$ downsampled latent states for both height and width, and 50 denoising steps.

Text extractor. We use Llama2-7B [48] to extract the background and object descriptions from the input prompt. The model is based on float-16. We set the maximum generated length as the maximum number of tokens that the diffusion model can process. To alleviate the overhead brought by this add-on module, we apply Flash Attention [11, 12] to speed up Llama execution.

Vector database. We use Qdrant [37] as the vector DB for cache lookup. FlexCache has three sets of prompt embeddings: object, background, and whole prompt, where each set of embeddings is kept in one index table. The query results of the vector database are pointers to the cache entry of the video latent states. Thus, even though we save three times as many indices, the total size of caches remains the same. For example, 700k unique prompts take 1000 GB to store their caches but all of the three types of embeddings only take 6 GB. Upon a new prompt, FlexCache save its background, object, and itself to the three index tables and set the value pointing to the same location in the storage. For the background similarity score and object similarity score, we choose the minimum value as the final score as this choice guarantees the quality of the generated video.

Cache compressor. We compress the video latent states using the method in Section 4.1. Figure 14a demonstrates the impact of different similarity thresholds (based on cosine similarity). Here we showcase three thresholds: 0.9, 0.95, and 0.99, and compress the latent of the 25th step. The result indicates that a threshold of 0.99 is necessary to guarantee high quality; lower thresholds lead to noticeable noise such as undesired patterns. Therefore, we take 0.99 as the threshold in our implementation. Figure 14b shows the percentage of redundant frames of each step with the similarity threshold of 0.99. As the step of the cache increases, the number of redundant frames reduces, as later steps contain more details.

Video segmenter. To achieve better segmentation results with given object and background prompts, we use

LangSAM [1] to figure out the boundaries of objects accurately. LangSAM is an open-source project that can perform instance segmentation and use text prompts to generate masks. Because it only works for images, we treat the whole video as a sequence of images and segment them to get masks for each frame. Since the masks only take 1 bit per pixel, saving the whole video’s masks is low-overhead but enables better stitching. Video segmentation is not on the critical path of FlexCache as it happens after the video has been generated. Besides, LangSAM is relatively lightweight. Therefore, we use the CPU to generate the mask, by starting another process to run the LangSAM-based segmentation while FlexCache processes new incoming prompts.

6 Evaluation

6.1 Evaluation Methodology

In this section, we discuss the methodology of our evaluation.

Platform. We evaluate the FlexCache on GCP machine type `a2-highgpu-1g` that comes with an Nvidia A100 40 GB GPU, 12 vCPU cores, and 85 GB main memory. We add an additional `balanced persistent disk` to store latent state caches. We compare the following video generation schemes:

- **No Cache:** Use the original model to directly generate videos, without caching prompts.
- **NIRVANA-video:** Directly adapt NIRVANA [3] to perform video caching, without cache compression, or decoupled object and background cache lookup.
- **FlexCache (this work):** Include all optimization techniques from Section 4.

Dataset. We evaluate FlexCache on dataset VidProM [52], which contains 1.67 M unique text-to-Video prompts from real-world users on Discord. Each prompt is associated with a timestamp. We select first 700 k prompts according to their timestamps for evaluation, which takes around 1000 GB of caching data. VidProM is similar to DiffusionDB, a commonly used text-to-image dataset [54] that is based on real-world users. However, VidProM has 40.6 % more semantically unique prompts, making cache reuse more challenging. Nonetheless, our evaluation of cache hit rate (Section 6.2.3) demonstrates that FlexCache enables a high hit rate using our hit rate optimization strategies.

Cache Replacement Policies. We evaluate the following cache replacement policies for video caching.

- **First In, First Out (FIFO):** Replace cache entries in the same order they were inserted, where the oldest entry gets evicted first.
- **Least Recently Used (LRU):** Replace the least recently used cache entry.
- **Least Computationally Beneficial and Frequently Used (LCBFU):** The replacement policy in NIRVANA [3] for

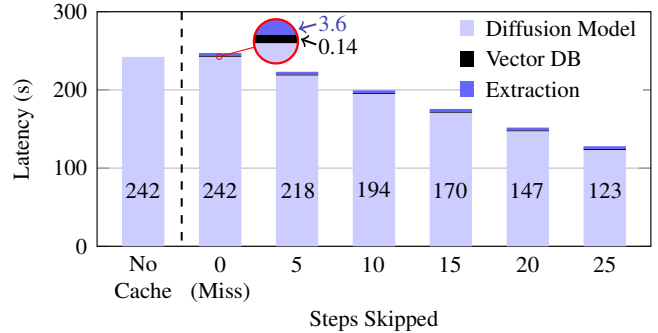


Figure 15: Latency breakdown.

image caching, as discussed in Section 4.2.3. We adapt this method to video caching.

- **Least Reused Benefit Unit (LRBU) in this work:** the replacement policy of FlexCache as introduced in Section 4.2.3.

Video Quality Metrics. We compare the video generation quality using the following metrics that are commonly used in evaluating video quality.

- **FVD [38]** calculate the distance between the generated video and the original video in dataset [50]. A lower FVD indicates the two videos are more similar. Typically, a difference of less than 50 between two generated video sets means the two sets have no visual difference [50].
- **CLIP-Text [23, 57]** get the average value of the cosine similarity scores between prompt and each frame in video [23]. A high score indicates better alignment between the video and the prompt.
- **CLIP-SIM [38, 41]** is generated by computing the average cosine similarity scores of the adjacent frames. A higher score indicates better quality [39, 42].

6.2 Evaluation Results

In this section, we evaluate the performance, generation quality, and cost of FlexCache.

6.2.1 Performance Breakdown

As discussed in Section 3.2, each prompt undergoes three main operations in FlexCache: extraction, vector DB lookup, and diffusion model. Figure 15 shows the latency breakdown (y-axis) when the prompt skips 0 (i.e., a cache miss), 5, 10, 15, 20, and 25 steps. In addition, we show the generation latency when no cache is used. We track the latency breakdown of 100 prompts and present the average. As the diffusion model is the most time-consuming, the bottom stack takes the majority of latency, ranging from 242 s to 123 s. We find that the latency reduction of the diffusion model is proportional to the skipped steps. In comparison, vector DB takes an average of 0.14 s — a latency visible only within the zoom-in circle. Extraction

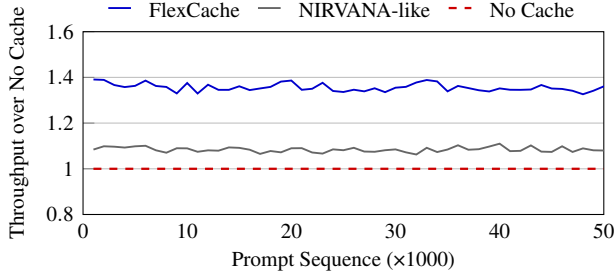


Figure 16: Throughput of video generation.

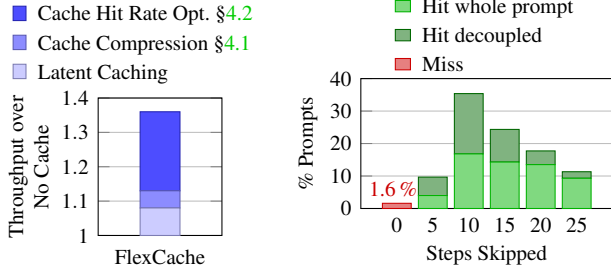


Figure 17: Breakdown of throughput gain. Figure 18: Distribution of number of steps skipped.

that uses Llama2-7B takes an average of 3.6 s. Nonetheless, this latency is only 1.5 % of the diffusion model.

6.2.2 Throughput Comparison

Throughput over time. This experiment demonstrates the throughput of video generation. We first set up a capacity limit of 1 TB and fill up the cache with prompts. Then, we evaluate 50k prompts according to their timestamps and record the generation throughput and cache hit rate, where we take the average value of every 1k prompts as one data point. Figure 16 shows the result, where the y-axis shows the throughput normalized to the “No Cache” baseline and the x-axis shows the prompt sequence. The result indicates that our system gets $1.26\times$ better throughput than NIRVANA-video on average.

Throughput Breakdown. Using the same setup as above, we break down the throughput improvements over the “No Cache” scheme, as Figure 17 shows. With latent caching alone, the improvement is $1.08\times$. By applying cache compression (Section 4.1) on top, the improvement becomes $1.13\times$. Finally, integrating the cache hit rate optimizations in FlexCache, including the LRBU replacement policy and decoupled object and background cache lookup improves the throughput to $1.36\times$ of the “No Cache” scenario.

Steps Skipped We next evaluate the cache hit rate by taking the same prompt sequence and capacity as Section 6.2.2. The y-axis in Figure 18 shows the percentage of prompts that skip 0, 5, 10, 15, 20, and 25 steps, where 0 step indicates a miss. Overall, the hit rate is 98.4 %, with skipping 10 steps being the most common (35.4 %).

Table 1: Comparison among cache replacement policies.

Policy	Cache Size	FIFO	LRU	LCBFU	LRBU
Hit Rate	1 GB	38 %	68 %	54 %	86 %
	10 GB	40 %	84 %	65 %	91 %
	100 GB	44 %	94 %	88 %	95 %
	1000 GB	48 %	98 %	97 %	98 %
Computation Savings	1 GB	10 %	15 %	13 %	18 %
	10 GB	11 %	19 %	15 %	21 %
	100 GB	14 %	23 %	20 %	24 %
	1000 GB	17 %	27 %	26 %	28 %

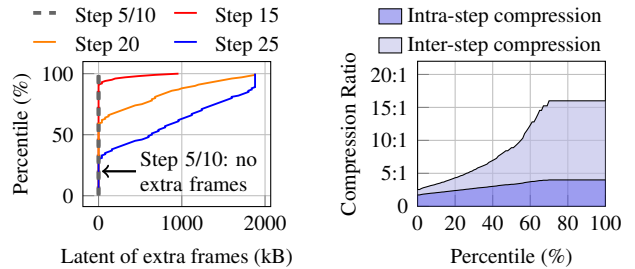


Figure 19: Size of latent of extra frames. Figure 20: Distribution of compression ratio.

6.2.3 Cache Replacement Comparison

LRBU is the default cache replacement policy in FlexCache. We perform a sensitivity study by replacing LRBU with other cache replacement policies in Section 6.1. We first initialize the cache to reach its size limit and then evaluate 50k prompts. Table 1 shows the hit rate and compute savings under cache sizes of 1 GB, 10 GB, 100 GB, and 1000 GB. Note that the computation savings measure the reduced diffusion model computations to reflect the correlation between the overall hit rate and actual skipped steps from each cache. As the cache capacity increases, the hit rate and computation savings also increase. Overall, LRBU has the highest computation savings among the four replacement policies.

6.2.4 Compression Efficiency and Quality

We conduct an experiment with latent states from 5k prompts to find the distribution of extra frames for different steps. Figure 19 demonstrates how the extra key frames change with steps. States from the 5th and 10th steps have no extra frames, while those later steps can have more frames. With the number of steps increasing, the latent state has a higher chance of having extra frames. Figure 20 shows the distribution of the compression ratio for these two compression techniques. We find that 31 % caches can achieve the highest $16\times$ compression ratio (when there are no extra frames); the worst-case 1 % caches can get the least $2.53\times$ compression ratio. Both compression techniques have similar compression ratio dis-

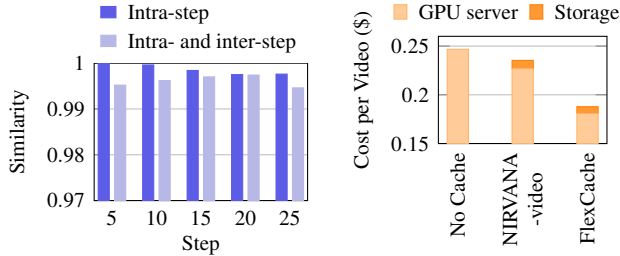


Figure 21: Quality of intra- and inter-step compression.

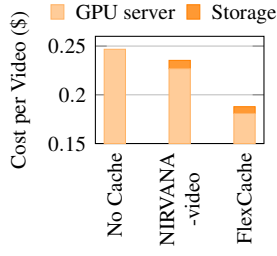


Figure 22: Cost of video generation.

Table 2: Quality comparison.

	FVD	CLIP-Text	CLIP-SIM
No Cache	168	0.25	0.94
FlexCache	192	0.24	0.92
NIRVANA-video	172	0.24	0.94

tributions as the reduction of compression ratio is due to the extra frames that are saved separated. On average, FlexCache reduces the cache size by $6.7\times$.

To evaluate the quality of compression, we first apply the intra-step compression and then apply the inter-step compression on top. Figure 21 shows the cosine similarity between the original, uncompressed latent state and the decompressed latent state. Both these two compression mechanisms only introduce little loss to the original cache. Overall, the similarity scores remain high (> 0.995), indicating a negligible difference in video quality.

6.2.5 Generation Quality

We compare the quality of generation using metrics in Section 6.1. We conduct an experiment with 2k videos to get all of those metrics. Similar to the approach in FreeNoise [38], we split the generated videos into multiple smaller videos to align frames in the generated with those in the reference video. Table 2 presents the quality metrics of FlexCache. In this table, we can find that all of these three metrics are highly acceptable. The FVD difference between FlexCache and the No Cache version is less than 50, which means such a difference in the quality of the generated videos that is hard to perceive by humans [50]. For the CLIP-Text and CLIP-SIM, there is also only a negligible difference as prior works have shown [51, 58].

6.2.6 Cost Savings

As our evaluation is based on GCP, we follow their pricing to estimate the cost savings from adopting FlexCache. The machine type `a2-highgpu-1g` costs 3.67\$/h and the storage balanced persistent disk for keeping video latent caches costs 0.1\$/GB every month (as of December

2024) [10]. We calculate the per-video cost when 1 TB of storage is used, as shown in Figure 22. Directly applying NIRVANA’s caching scheme to video only yields 4.8 % savings as compared to No Cache, as the additional storage cost offsets the savings. In comparison, FlexCache has significant cost savings of 31 %.

7 Discussions and Related Works

Diffusion Model Optimizations. There are multiple researches that focus on improving the performance of diffusion models. DeepCache [32], Block Caching [55], and Learning-to-Cache [31] discover that the outputs of layers among multiple steps are similar, so they can cache the output from the last step and reuse it in the current step. FISEdit [60] finds that users tend to change only a little in the same session. It saves all the intermediate outputs from all model layers and steps. When the next request in the same session arrives, it attempts to reuse the existing outputs. These proposals can speed up diffusion models but are orthogonal to FlexCache as they do not change the number of denoising steps. However, it is possible to integrate these optimizations into FlexCache to further reduce the video generation time.

Approximate Caching for image diffusion models. NIRVANA [3] is the state-of-the-art approximate caching system for image diffusion models. While it is good in image generation, we have shown that it is not efficient in video generation.

Support for other models. As far as we know, FlexCache is the first approximate caching system for text-to-video diffusion models. For evaluation, we integrated VideoCrafter2 [7] as the diffusion model. Other diffusion models can be supported. Moreover, other diffusion-based generation tasks [5, 8, 45, 58] can also leverage our caching scheme.

Creativity of generation. Since FlexCache reuses the cache from the previous request and achieves a relatively high hit rate, the generated videos may tend to be less diverse over time. To alleviate this homogenization, FlexCache deploy the same strategy as NIRVANA [3] that changes the denoising seed after retrieval.

8 Conclusions

In this paper, we introduce the motivation and design of FlexCache which further optimizes the approximate cache method for video generation. We compress the cache size to accommodate more caches under a fixed storage. Then we decouple the background and object for more efficient cache lookup, achieving higher hit rate and more computation savings. We also provide a cache replacement policy tailored to the two designs above. Finally, the evaluation shows that our system can gain $1.26\times$ throughput and 25 % cost savings over NIRVANA’s approximate caching system.

References

- [1] Language segment-anything. <https://github.com/luca-medeiros/lang-segment-anything>, 2024.
- [2] Adobe. Create with adobe firefly generative AI. <https://www.adobe.com/products/firefly.html>, 2023.
- [3] Shubham Agarwal, Subrata Mitra, Sarthak Chakraborty, Srikrishna Karanam, Koyel Mukherjee, and Shiv Kumar Saini. Approximate caching for efficiently serving Text-to-Image diffusion models. In *21st USENIX Symposium on Networked Systems Design and Implementation (NSDI 24)*, pages 1173–1189, Santa Clara, CA, April 2024. USENIX Association.
- [4] Yongqi An, Xu Zhao, Tao Yu, Haiyun Gu, Chaoyang Zhao, Ming Tang, and Jinqiao Wang. ZBS: Zero-shot background subtraction via instance-level background modeling and foreground selection. In *IEEE/CVF Conference on Computer Vision and Pattern Recognition (CVPR)*, pages 6355–6364, 2023.
- [5] Andreas Blattmann, Tim Dockhorn, Sumith Kulal, Daniel Mendelevitch, Maciej Kilian, Dominik Lorenz, Yam Levi, Zion English, Vikram Voleti, Adam Letts, Varun Jampani, and Robin Rombach. Stable video diffusion: Scaling latent video diffusion models to large datasets, 2023.
- [6] Daniel Bolya and Judy Hoffman. Token merging for fast stable diffusion. In *Proceedings of the IEEE/CVF Conference on Computer Vision and Pattern Recognition (CVPR) Workshops*, pages 4599–4603, June 2023.
- [7] Haoxin Chen, Yong Zhang, Xiaodong Cun, Menghan Xia, Xintao Wang, Chao Weng, and Ying Shan. VideoCrafter2: Overcoming data limitations for high-quality video diffusion models. In *IEEE/CVF Conference on Computer Vision and Pattern Recognition (CVPR)*, pages 7310–7320, 2024.
- [8] Shoufa Chen, Mengmeng Xu, Jiawei Ren, Yuren Cong, Sen He, Yanping Xie, Animesh Sinha, Ping Luo, Tao Xiang, and Juan-Manuel Perez-Rua. Gentrion: Diffusion transformers for image and video generation. In *Proceedings of the IEEE/CVF Conference on Computer Vision and Pattern Recognition (CVPR)*, pages 6441–6451, June 2024.
- [9] Mengjun Cheng, Chengquan Zhang, Chang Liu, Yuke Li, Bohan Li, Kun Yao, Xiawu Zheng, Rongrong Ji, and Jie Chen. Textual grounding for open-vocabulary visual information extraction in layout-diversified documents. In Aleš Leonardis, Elisa Ricci, Stefan Roth, Olga Russakovsky, Torsten Sattler, and Gül Varol, editors, *Proceedings of the European Conference on Computer Vision (ECCV)*, pages 474–491, Cham, 2025. Springer Nature Switzerland.
- [10] Google Cloud. Compute engine pricing. <https://cloud.google.com/compute/all-pricing>, 2024.
- [11] Tri Dao. FlashAttention-2: Faster attention with better parallelism and work partitioning. In *International Conference on Learning Representations (ICLR)*, 2024.
- [12] Tri Dao, Daniel Y. Fu, Stefano Ermon, Atri Rudra, and Christopher Ré. FlashAttention: Fast and memory-efficient exact attention with IO-awareness. In *Advances in Neural Information Processing Systems (NeurIPS)*, 2022.
- [13] DeepMind. Veo: Our most capable generative video model. <https://deepmind.google/technologies/veo>, 2024.
- [14] Prafulla Dhariwal and Alexander Nichol. Diffusion models beat gans on image synthesis. In M. Ranzato, A. Beygelzimer, Y. Dauphin, P.S. Liang, and J. Wortman Vaughan, editors, *Advances in Neural Information Processing Systems (NeurIPS)*, volume 34, pages 8780–8794. Curran Associates, Inc., 2021.
- [15] Abdelaziz Djelouah, Joaquim Campos, Simone Schaub-Meyer, and Christopher Schroers. Neural inter-frame compression for video coding. In *Proceedings of the IEEE/CVF International Conference on Computer Vision (ICCV)*, October 2019.
- [16] Jiarui Fang, Jinzhe Pan, Xibo Sun, Aoyu Li, and Jiannan Wang. xdit: an inference engine for diffusion transformers (dits) with massive parallelism, 2024.
- [17] Hao Fei, Shengqiong Wu, Wei Ji, Hanwang Zhang, and Tat-Seng Chua. Dysen-VDM: Empowering dynamics-aware text-to-video diffusion with llms. In *IEEE/CVF Conference on Computer Vision and Pattern Recognition (CVPR)*, pages 7641–7653, 2024.
- [18] In Gim, Guojun Chen, Seung-seob Lee, Nikhil Sarda, Anurag Khandelwal, and Lin Zhong. Prompt cache: Modular attention reuse for low-latency inference. In P. Gibbons, G. Pekhimenko, and C. De Sa, editors, *Proceedings of Machine Learning and Systems (MLSys)*, volume 6, pages 325–338, 2024.
- [19] Jonathan Ho, Ajay Jain, and Pieter Abbeel. Denoising diffusion probabilistic models. In H. Larochelle, M. Ranzato, R. Hadsell, M.F. Balcan, and H. Lin, editors, *Advances in Neural Information Processing Systems (NeurIPS)*, volume 33, pages 6840–6851. Curran Associates, Inc., 2020.

- [20] Edward J Hu, yelong shen, Phillip Wallis, Zeyuan Allen-Zhu, Yuanzhi Li, Shean Wang, Lu Wang, and Weizhu Chen. LoRA: Low-rank adaptation of large language models. In *International Conference on Learning Representations (ICLR)*, 2022.
- [21] Hyeonho Jeong, Geon Yeong Park, and Jong Chul Ye. VMC: Video motion customization using temporal attention adaption for text-to-video diffusion models. In *2024 IEEE/CVF Conference on Computer Vision and Pattern Recognition (CVPR)*, pages 9212–9221, 2024.
- [22] Hyeonho Jeong and Jong Chul Ye. Ground-a-video: Zero-shot grounded video editing using text-to-image diffusion models. In *The Twelfth International Conference on Learning Representations (ICLR)*, 2024.
- [23] Yuming Jiang, Tianxing Wu, Shuai Yang, Chenyang Si, Dahua Lin, Yu Qiao, Chen Change Loy, and Ziwei Liu. VideoBooth: Diffusion-based video generation with image prompts. In *IEEE/CVF Conference on Computer Vision and Pattern Recognition (CVPR)*, pages 6689–6700, 2024.
- [24] Kling. Kling ai: Next-generation ai creative studio. <https://klingai.com/>, 2024.
- [25] Weihao Kong, Yifan Hao, Qi Guo, Yongwei Zhao, Xinkai Song, Xiqing Li, Mo Zou, Zidong Du, Rui Zhang, Chang Liu, Yuanbo Wen, Pengwei Jin, Xing Hu, Wei Li, Zhiwei Xu, and Tianshi Chen. Cambricon-d: Full-network differential acceleration for diffusion models. In *2024 ACM/IEEE 51st Annual International Symposium on Computer Architecture (ISCA)*, pages 903–914, 2024.
- [26] Benjamin Lefaudeux, Francisco Massa, Diana Liskovich, Wenhan Xiong, Vittorio Caggiano, Sean Naren, Min Xu, Jieru Hu, Marta Tintore, Susan Zhang, Patrick Labatut, Daniel Haziza, Luca Wehrstedt, Jeremy Reizenstein, and Grigory Sizov. xformers: A modular and hackable transformer modelling library. <https://github.com/facebookresearch/xformers>, 2022.
- [27] Hao Li, Yang Zou, Ying Wang, Orchid Majumder, Yusheng Xie, R. Manmatha, Ashwin Swaminathan, Zhuowen Tu, Stefano Ermon, and Stefano Soatto. On the scalability of diffusion-based text-to-image generation. In *2024 IEEE/CVF Conference on Computer Vision and Pattern Recognition (CVPR)*, pages 9400–9409, 2024.
- [28] Muyang Li, Tianle Cai, Jiaxin Cao, Qinsheng Zhang, Han Cai, Junjie Bai, Yangqing Jia, Kai Li, and Song Han. Distrifusion: Distributed parallel inference for high-resolution diffusion models. In *Proceedings of the IEEE/CVF Conference on Computer Vision and Pattern Recognition (CVPR)*, pages 7183–7193, June 2024.
- [29] Suyi Li, Lingyun Yang, Xiaoxiao Jiang, Hanfeng Lu, Zhipeng Di, Weiyi Lu, Jiawei Chen, Kan Liu, Yinghao Yu, Tao Lan, Guodong Yang, Lin Qu, Liping Zhang, and Wei Wang. SwiftDiffusion: Efficient diffusion model serving with add-on modules, 2024.
- [30] Cheng Lu, Yuhao Zhou, Fan Bao, Jianfei Chen, Chongxuan Li, and Jun Zhu. DPM-Solver++: Fast solver for guided sampling of diffusion probabilistic models. In *The Eleventh International Conference on Learning Representations (ICLR)*, 2023.
- [31] Xinyin Ma, Gongfan Fang, Michael Bi Mi, and Xinchao Wang. Learning-to-cache: Accelerating diffusion transformer via layer caching, 2024.
- [32] Xinyin Ma, Gongfan Fang, and Xinchao Wang. Deep-cache: Accelerating diffusion models for free. In *2024 IEEE/CVF Conference on Computer Vision and Pattern Recognition (CVPR)*, pages 15762–15772, 2024.
- [33] OpenAI. Video generation models as world simulators. <https://openai.com/index/video-generation-models-as-world-simulators>, 2024.
- [34] Adam Paszke, Sam Gross, Francisco Massa, Adam Lerer, James Bradbury, Gregory Chanan, Trevor Killeen, Zeming Lin, Natalia Gimelshein, Luca Antiga, Alban Desmaison, Andreas Köpf, Edward Yang, Zach DeVito, Martin Raison, Alykhan Tejani, Sasank Chilamkurthy, Benoit Steiner, Lu Fang, Junjie Bai, and Soumith Chintala. PyTorch: an imperative style, high-performance deep learning library. In *Proceedings of the 33rd International Conference on Neural Information Processing Systems (NeurIPS)*, Red Hook, NY, USA, 2019. Curran Associates Inc.
- [35] William Peebles and Saining Xie. Scalable diffusion models with transformers. In *IEEE/CVF International Conference on Computer Vision (ICCV)*, pages 4172–4182, 2023.
- [36] Dustin Podell, Zion English, Kyle Lacey, Andreas Blattmann, Tim Dockhorn, Jonas Müller, Joe Penna, and Robin Rombach. SDXL: Improving latent diffusion models for high-resolution image synthesis. In *The Twelfth International Conference on Learning Representations (ICLR)*, 2024.
- [37] Qdrant. vector database. <https://qdrant.tech/>, 2023.
- [38] Haonan Qiu, Menghan Xia, Yong Zhang, Yingqing He, Xintao Wang, Ying Shan, and Ziwei Liu. Freenoise: Tuning-free longer video diffusion via noise rescheduling. In *The Twelfth International Conference on Learning Representations (ICLR)*, 2024.

- [39] Haonan Qiu, Menghan Xia, Yong Zhang, Yingqing He, Xintao Wang, Ying Shan, and Ziwei Liu. Freenoise: Tuning-free longer video diffusion via noise rescheduling. In *The Twelfth International Conference on Learning Representations (ICLR)*, 2024.
- [40] Alec Radford, Jong Wook Kim, Chris Hallacy, Aditya Ramesh, Gabriel Goh, Sandhini Agarwal, Girish Sastry, Amanda Askell, Pamela Mishkin, Jack Clark, Gretchen Krueger, and Ilya Sutskever. Learning transferable visual models from natural language supervision. In Marina Meila and Tong Zhang, editors, *Proceedings of the 38th International Conference on Machine Learning (ICML)*, volume 139 of *Proceedings of Machine Learning Research*, pages 8748–8763. PMLR, 18–24 Jul 2021.
- [41] Alec Radford, Jong Wook Kim, Chris Hallacy, Aditya Ramesh, Gabriel Goh, Sandhini Agarwal, Girish Sastry, Amanda Askell, Pamela Mishkin, Jack Clark, Gretchen Krueger, and Ilya Sutskever. Learning transferable visual models from natural language supervision. In Marina Meila and Tong Zhang, editors, *Proceedings of the 38th International Conference on Machine Learning (ICML)*, volume 139 of *Proceedings of Machine Learning Research*, pages 8748–8763. PMLR, 18–24 Jul 2021.
- [42] Alec Radford, Jong Wook Kim, Chris Hallacy, Aditya Ramesh, Gabriel Goh, Sandhini Agarwal, Girish Sastry, Amanda Askell, Pamela Mishkin, Jack Clark, Gretchen Krueger, and Ilya Sutskever. Learning transferable visual models from natural language supervision. In Marina Meila and Tong Zhang, editors, *Proceedings of the 38th International Conference on Machine Learning (ICML)*, volume 139 of *Proceedings of Machine Learning Research*, pages 8748–8763. PMLR, 18–24 Jul 2021.
- [43] Robin Rombach, Andreas Blattmann, Dominik Lorenz, Patrick Esser, and Björn Ommer. High-resolution image synthesis with latent diffusion models. In *IEEE/CVF Conference on Computer Vision and Pattern Recognition (CVPR)*, pages 10674–10685, 2022.
- [44] Olaf Ronneberger, Philipp Fischer, and Thomas Brox. U-net: Convolutional networks for biomedical image segmentation. In *Medical image computing and computer-assisted intervention (MICCAI)*, pages 234–241. Springer, 2015.
- [45] Uriel Singer, Adam Polyak, Thomas Hayes, Xi Yin, Jie An, Songyang Zhang, Qiyuan Hu, Harry Yang, Oron Ashual, Oran Gafni, Devi Parikh, Sonal Gupta, and Yaniv Taigman. Make-a-video: Text-to-video generation without text-video data. In *The Eleventh International Conference on Learning Representations (ICLR)*, 2023.
- [46] Jiaming Song, Chenlin Meng, and Stefano Ermon. Denoising diffusion implicit models. In *International Conference on Learning Representations (ICLR)*, 2021.
- [47] Lin Sun, Kai Zhang, Qingyuan Li, and Renze Lou. Umie: Unified multimodal information extraction with instruction tuning. In *Proceedings of the AAAI Conference on Artificial Intelligence (AAAI)*, 2024.
- [48] Hugo Touvron, Louis Martin, Kevin Stone, Peter Albert, Amjad Almahairi, Yasmine Babaei, Nikolay Bashlykov, Soumya Batra, Prajjwal Bhargava, Shruti Bhosale, Dan Bikel, Lukas Blecher, Cristian Canton Ferrer, Moya Chen, Guillem Cucurull, David Esiobu, Jude Fernandes, Jeremy Fu, Wenyin Fu, Brian Fuller, Cynthia Gao, Vedanuj Goswami, Naman Goyal, Anthony Hartshorn, Saghar Hosseini, Rui Hou, Hakan Inan, Marcin Kardas, Viktor Kerkez, Madian Khabsa, Isabel Kloumann, Artem Korenev, Punit Singh Koura, Marie-Anne Lachaux, Thibaut Lavril, Jenya Lee, Diana Liskovich, Yinghai Lu, Yuning Mao, Xavier Martinet, Todor Mihaylov, Pushkar Mishra, Igor Molybog, Yixin Nie, Andrew Poulton, Jeremy Reizenstein, Rashi Rungta, Kalyan Saladi, Alan Schelten, Ruan Silva, Eric Michael Smith, Ranjan Subramanian, Xiaoqing Ellen Tan, Binh Tang, Ross Taylor, Adina Williams, Jian Xiang Kuan, Puxin Xu, Zheng Yan, Iliyan Zarov, Yuchen Zhang, Angela Fan, Melanie Kambadur, Sharan Narang, Aurelien Rodriguez, Robert Stojnic, Sergey Edunov, and Thomas Scialom. Llama 2: Open foundation and fine-tuned chat models, 2023.
- [49] Yunbin Tu, Xishan Zhang, Bingtao Liu, and Chenggang Yan. Video description with spatial-temporal attention. In *Proceedings of the 25th ACM International Conference on Multimedia (ACM Multimedia)*, MM '17, page 1014–1022, New York, NY, USA, 2017. Association for Computing Machinery.
- [50] Thomas Unterthiner, Sjoerd van Steenkiste, Karol Kurach, Raphaël Marinier, Marcin Michalski, and Sylvain Gelly. FVD: A new metric for video generation. In *International Conference on Learning Representations (ICLR)*, 2019.
- [51] Fu-Yun Wang, Zhaoyang Huang, Qiang Ma, Guanglu Song, Xudong Lu, Weikang Bian, Yijin Li, Yu Liu, and Hongsheng Li. ZoLA: Zero-shot creative long animation generation with short video model. In Aleš Leonardis, Elisa Ricci, Stefan Roth, Olga Russakovsky, Torsten Sattler, and Gül Varol, editors, *Proceedings of the European Conference on Computer Vision (ECCV)*, pages 329–345, Cham, 2025. Springer Nature Switzerland.
- [52] Wenhao Wang and Yi Yang. Vidprom: A million-scale real prompt-gallery dataset for text-to-video diffusion models, 2024.

- [53] Wenjing Wang, Huan Yang, Zixi Tuo, Huiguo He, Junchen Zhu, Jianlong Fu, and Jiaying Liu. Videofactory: Swap attention in spatiotemporal diffusions for text-to-video generation. In *The Twelfth International Conference on Learning Representations (ICLR)*, 2024.
- [54] Zijie J. Wang, Evan Montoya, David Munechika, Haoyang Yang, Benjamin Hoover, and Duen Horng Chau. DiffusionDB: A large-scale prompt gallery dataset for text-to-image generative models. In Anna Rogers, Jordan Boyd-Graber, and Naoaki Okazaki, editors, *Proceedings of the 61st Annual Meeting of the Association for Computational Linguistics (Volume 1: Long Papers) (ACL)*, pages 893–911, Toronto, Canada, July 2023. Association for Computational Linguistics.
- [55] Felix Wimbauer, Bichen Wu, Edgar Schoenfeld, Xiaoliang Dai, Ji Hou, Zijian He, Artsiom Sanakoyeu, Peizhao Zhang, Sam Tsai, Jonas Kohler, Christian Rupprecht, Daniel Cremers, Peter Vajda, and Jialiang Wang. Cache me if you can: Accelerating diffusion models through block caching. In *IEEE/CVF Conference on Computer Vision and Pattern Recognition (CVPR)*, pages 6211–6220, 2024.
- [56] Chao-Yuan Wu, Nayan Singhal, and Philipp Krahenbuhl. Video compression through image interpolation. In *Proceedings of the European Conference on Computer Vision (ECCV)*, September 2018.
- [57] Jay Zhangjie Wu, Guian Fang, Haoning Wu, Xintao Wang, Yixiao Ge, Xiaodong Cun, David Junhao Zhang, Jia-Wei Liu, Yuchao Gu, Rui Zhao, Weisi Lin, Wynne Hsu, Ying Shan, and Mike Zheng Shou. Towards a better metric for text-to-video generation, 2024.
- [58] Jinbo Xing, Menghan Xia, Yong Zhang, Haoxin Chen, Wangbo Yu, Hanyuan Liu, Gongye Liu, Xintao Wang, Ying Shan, and Tien-Tsin Wong. DynamiCrafter: Animating open-domain images with video diffusion priors. In Aleš Leonardis, Elisa Ricci, Stefan Roth, Olga Russakovsky, Torsten Sattler, and Gül Varol, editors, *Proceedings of the European Conference on Computer Vision (ECCV)*, pages 399–417, Cham, 2025. Springer Nature Switzerland.
- [59] Fulong Ye, Guang Liu, Xinya Wu, and Ledell Wu. Alt-diffusion: A multilingual text-to-image diffusion model. *Proceedings of the AAAI Conference on Artificial Intelligence (AAAI)*, 38(7):6648–6656, Mar. 2024.
- [60] Zihao Yu, Haoyang Li, Fangcheng Fu, Xupeng Miao, and Bin Cui. Accelerating text-to-image editing via cache-enabled sparse diffusion inference. *Proceedings of the AAAI Conference on Artificial Intelligence (AAAI)*, 38(15):16605–16613, Mar. 2024.
- [61] Lvmin Zhang, Anyi Rao, and Maneesh Agrawala. Adding conditional control to text-to-image diffusion models. In *2023 IEEE/CVF International Conference on Computer Vision (ICCV)*, pages 3813–3824, 2023.
- [62] Shen Zhang, Zhaowei Chen, Zhenyu Zhao, Yuhao Chen, Yao Tang, and Jiajun Liang. Hidiffusion: Unlocking higher-resolution creativity and efficiency in pretrained diffusion models. In Aleš Leonardis, Elisa Ricci, Stefan Roth, Olga Russakovsky, Torsten Sattler, and Gül Varol, editors, *Proceedings of the European Conference on Computer Vision (ECCV)*, pages 145–161, Cham, 2025. Springer Nature Switzerland.